Fission properties of the Barcelona-Catania-Paris-Madrid energy density functional

Samuel A. Giuliani* and Luis M. Robledo†
Departamento de Física Teórica, Universidad Autónoma de Madrid, E-28049 Madrid, Spain
(Received 26 August 2013; revised manuscript received 21 October 2013; published 27 November 2013)

Fission dynamics properties of the Barcelona-Catania-Paris-Madrid energy density functional are explored with mean-field techniques. Potential energy surfaces as well as collective inertias relevant in the fission process are computed for several nuclei where experimental data exist. Inner and outer barrier heights as well as fission isomer excitation energies are reproduced quite well in all the cases. The spontaneous fission half-lives t_{sf} are also computed using the standard semiclassical approach and the results are compared with the experimental data. The experimental trend with mass number is reasonably well reproduced over a range of 27 orders of magnitude. However, the theoretical predictions suffer from large uncertainties when the quantities that enter the spontaneous fission half-life formula are varied. Modifications of only a few per cent in the pairing correlation strengths strongly modify the collective inertias with a large impact on the spontaneous fission lifetimes in all the nuclei considered. Encouraged by the quite satisfactory description of the trend of fission properties with mass number, we explore the fission properties of the even-even uranium isotope chain from ^{226}U to ^{282}U. Very large lifetimes are found beyond $A = 256$ with a peak at neutron number $N = 184$.

DOI: 10.1103/PhysRevC.88.054325 PACS number(s): 24.75.+i, 21.10.Tg, 25.85.Ca, 27.90.+b

I. INTRODUCTION

Fission is a physical phenomenon taking place in heavy atomic nuclei that leads to the disintegration of a parent nucleus into two or more emerging fragments. It involves the evolution of the nucleus from its ground state to scission going through a variety of intrinsic shapes covering a wide range of different intrinsic deformation parameters [1–4]. Fission properties depend upon the competition between the surface energy term coming from the strong nuclear interaction and the Coulomb repulsion and therefore they are often used as constraints and/or guidance to refine the parameters of effective nuclear interactions. A typical example is the D1S parametrization of the Gogny [5] force with parameters fine-tuned to reproduce the fission barrier of ^{240}Pu [6]. For Skyrme forces, the SkM* parametrization [7] is a typical example of an interaction fitted to fission properties. More recently, fission-related constraints have been used with Skyrme interactions to define the UNEDF1 parametrization [8,9] that, unlike SkM*, also performs well with binding energies.

The gross features of fission can be understood from a mean-field perspective using the Hartree-Fock-Bogoliubov (HFB) theory [10] and therefore the large amount of studies devoted to this subject with Skyrme interactions [9,11–13] or Gogny ones [6,14–21] or based on the relativistic mean field [22–24] is not surprising. Fission observables also depend on the inertia of the system to the relevant collective degrees of freedom and therefore they are sensitive to pairing correlations. As a consequence, fission is a good testing ground for both the theories and interactions commonly used in nuclear structure to describe pairing correlations. In addition, an improved theoretical understanding of fission would be relevant to other areas outside traditional nuclear physics like safe energy production with nuclear reactors, radioactive waste degradation, or the synthesis through the r-process of heavy elements in the explosive galactic environments [25,26]. Last but not least, a better understanding of fission could open the door to a better estimation of magic numbers and, hence, extra stability of superheavy nuclei beyond $Z = 114$. In this paper we explore the ability of a newly proposed energy density functional (EDF), denoted as Barcelona-Catania-Paris-Madrid (BCPM) [27], to describe fission.

The BCPM is a recent parametrization of the BCP EDF [28–31] devised for nuclear structure calculations. Its free parameters have been adjusted to reproduce the binding energies of all known even-even nuclei, including deformed ones. Instead of the more traditional approaches where some central potential form is guessed (contact, Gaussian, Yukawa, etc.) and used afterwards to fit nuclear matter properties and/or the nuclear matter equations of state EOS (both symmetric and neutron), in the BCPM functional we start from a microscopic EOS that is fitted by means of a low-order polynomial in the density. That polynomial fit is translated to a finite nuclei EDF just by replacing the nuclear matter density by the density of the finite nucleus. This procedure is inspired by the local density approximation (LDA) and is common practice in practical applications of the Kohn-Sham theory in condensed matter physics. The EDF is supplemented with a finite-range surface term, a contact spin-orbit interaction of the same form as in Skyrme or Gogny forces, the Coulomb interaction, and, finally, a density-dependent zero-range pairing interaction [32] with strengths fitted to reproduce Gogny's neutron matter pairing gap. The parameters of the functional (essentially those of the finite range surface term plus some freedom in the polynomial fit to fine tune the binding energy per nucleon) are fitted to reproduce binding energies of the 518 even-even nuclei of the 2003 mass table evaluation of Audi and Wapstra. The properties of the interaction concerning quadrupole, octupole, and fission dynamics have also been explored [27]. As shown below, the BCPM functional gives reasonable results for fission

*sam.and.giuliani@gmail.com
†luis.robledo@uam.es

observables, including spontaneous fission half-lives, fission isomer excitation energies, inner and outer barrier heights, and mass distribution of fragments. We have also shown that those results could be improved by slightly modifying the amount of pairing correlations, either by modifying the pairing strengths or by going beyond the mean-field approximation to restore the particle number symmetry broken by the HFB procedure. As a consequence of the satisfactory performance of BCPM in describing fission, we have explored fission properties of the uranium isotopic chain from proton drip line to the neutron drip line.

II. METHODS

Both the BCPM energy density functional [27] and its predecessor BCP [28] contain a bulk part which is determined by fully microscopic and realistic calculations of symmetric and neutron matter equations of state [33,34] as in the LDA of condensed matter physics. The two equations of state (symmetric and neutron matter), given as a function of the nuclear density, are parametrized by low order polynomials of the densities. To account for finite-size effects related to the surface energy, a phenomenological finite-range Gaussian interaction is included. In addition, the Coulomb interaction and the spin-orbit term are taken exactly as in the Skyrme or Gogny forces. To deal with open-shell nuclei we include in the BCPM and BCP functionals a zero-range density-dependent pairing interaction fitted to reproduce the nuclear matter gaps obtained with the Gogny force [32]. The calculations in finite nuclei are carried out with a modification of the HFBAXIAL computer code developed by one of the authors [35].

To describe fission we follow the usual procedure based on the mean-field approach with pairing correlations: the Hartree-Fock-Bogoliubov (HFB) theory with constraints [10]. As constraint operators we have used mainly the axially symmetric quadrupole moment operator $Q_{20} = z^2 - \frac{1}{2}(x^2 + y^2)$, although some exploratory calculations have also been performed with the octupole Q_{30} and hexadecapole Q_{40} moment operators and the necking operator $Q_N(z_0, C_0) = \exp[-(z - z_0)^2/C_0^2]$. Axial symmetry is preserved in the calculations because of the high computational cost of releasing this restriction. We are aware of the relevance of triaxiality especially in the height of the inner fission barrier but its effect is merely quantitative and, to a much lesser extent, qualitative. On the other hand, reflection symmetry is allowed to break at any stage of the calculation permitting octupole deformation and asymmetric fission. As a consequence of the breaking of the parity symmetry we are forced to constraint the center of mass to the origin as to prevent spurious translational motion of the nucleus as a whole. The quasiparticle creation and annihilation operators of the HFB theory are expanded in a harmonic oscillator basis (HO) preserving axial symmetry and containing HO states with J_z quantum numbers up to $35/2\ \hbar$ and up to 26 quanta in the z direction. The basis contains over 3000 levels but time-reversal invariance and the axial block structure reduces the computational complexity to a manageable level. The two lengths characterizing the HO basis, $b_\perp$ and b_z, have been optimized in a few nuclei for each value of the quadrupole moment. For the others the oscillator lengths computed for nearby nuclei are used. This optimization procedure guarantees a good convergence for relative energies. As the number of HFB configurations for each nucleus is large, a robust and fast gradient-like algorithm to solve the HFB equations is used [10,36]. The most evident advantage of this method is the way it handles the constraints, which allows an easy generalization to an arbitrary number of them.

The spontaneous fission lifetime formulas Eqs (4) and (5) below depend crucially on the theory of the collective mass $B(Q_{20})$. We shall use two methods to calculate it and compare in our results. The first is the well-known cranking approximation to the adiabatic-time-dependent HFB approximation [10]. The resulting mass is expressed in terms of the moments $M_{(-n)}$ of the generating field Q_{20},

$$M_{(-n)} = \sum_{\alpha>\beta} \langle 0|Q_{20}|\alpha\beta\rangle \frac{1}{(E_\alpha + E_\beta)^n} \langle \alpha\beta|Q_{20}|0\rangle \tag{1}$$

as [37–39]

$$B(Q_{20}) = \frac{1}{2}\frac{M_{-3}}{(M_{-1})^2}. \tag{2}$$

Here $|\alpha\beta\rangle$ are distinct two-quasiparticle excitations and $E_\alpha + E_\beta$ is the excitation energy, neglecting the quasiparticle-quasiparticle interaction (cranking approximation [37–39]).

An alternative method to calculate the mass is based on the Gaussian overlap approximation to the generator coordinate method (GCM). It is often simplified to obtain the expression [10]

$$B(Q_{20}) = \frac{1}{2}\frac{M_{-2}^2}{(M_{-1})^3}. \tag{3}$$

We shall calculate the lifetimes with both Eqs. (2) and (3) and compare. We note that Ref. [40] compares several forms of the mass, including Eqs. (2) and (3), in the context of the Skyrme functionals. It is also important to mention the dependence of the mass with the amount of pairing correlations: It has been shown in Refs. [4,41] that the mass is inversely proportional to the square of the pairing gap. It means that the stronger the pairing correlations, the smaller the mass.

Zero-point energy corrections to the HFB energy $\epsilon_0(Q_{20})$ are also considered in the ATDHFB and GCM approaches. In addition, the rotational energy correction computed following the phenomenological prescription of Ref. [42] is also subtracted. This correction is very important to the shape of the potential energy, as its value increases with deformation and can reach several MeV for large deformations.

The spontaneous fission half-life is computed with the standard WKB formalism of quantum mechanics. In the WKB formalism the $t_{\rm sf}$ is given (in seconds) by the formula (see Ref. [4] for a discussion in the present context)

$$t_{\rm sf} = 2.86\,10^{-21}[1 + \exp(2S)]. \tag{4}$$

The action S along the Q_{20} constrained path is given by

$$S = \int_a^b dQ_{20}\sqrt{2B(Q_{20})(V(Q_{20}) - (E_{\rm GS} + E_{0)})}, \tag{5}$$

where the integration limits a and b correspond to the classical turning points which are determined by the condition $V(Q_{20}) - E_{\rm GS} - E_0 = 0$. For the collective quadrupole inertia $B(Q_{20})$ we have used both the ATDHFB and the GCM expressions. The results obtained with the two different theories can differ in several orders of magnitude as the ATDHFB mass is known to be a factor in between 1.5 and 2 larger than the GCM mass. The potential energy $V(Q_{20})$ is given by the HFB mean-field energy corrected by zero-point energies as described above, $V(Q_{20}) = E_{\rm HFB}(Q_{20}) - \epsilon_0(Q_{20}) - E_{\rm Rot}(Q_{20})$. Finally, an additional parameter, E_0, is added to the ground-state energy $E_{\rm GS}$. It is meant to represent the true ground-state energy obtained after considering quantal fluctuations in the quadrupole degree of freedom. This quantity could be estimated to be half of the square root of the curvature around the minimum divided by the collective inertia but it is often taken as a free parameter or kept fixed at some reasonable value. We have followed the latter approach with $E_0 = 1.0$ MeV and estimated the impact of considering a larger value by repeating the calculations with $E_0 = 1.5$ MeV. The present framework has also been successfully applied to the description of cluster emission as a highly asymmetric fission process where the octupole moment is the relevant degree of freedom [43].

The above expressions assume that the quadrupole moment is the only relevant degree of freedom for fission. If other degrees of freedom Q_i were to be considered, the inertia should be replaced by the standard formula [4,44]

$$B(s) = \sum_{i,j} B_{i,j} \frac{dQ_i}{ds} \frac{dQ_j}{ds}, \tag{6}$$

where s represents a path in the multidimensional energy surface. We have checked in our case that the contributions of the octupole and hexadecapole degrees of freedom to the above expression of the inertia are small.

The spontaneous fission half-life obtained in this way is subject to several uncertainties that can lead to differences of several orders of magnitude. The uncertainties are as follows. (1) The height of the inner fission barrier gets reduced when triaxial shapes are allowed in the mean-field calculation. The amount of reduction is typically of a couple of MeV, but it can show some isotopic modulation (see Ref. [17] for a recent account in the actinide region). (2) The value of E_0 influences $t_{\rm sf}$ especially for long-lived isotopes where the fission barrier is wide. The reason is that the value of E_0 shifts the classical turning points. (3) The values of the correlation energy corrections to the HFB energy included in $V(Q_{20})$ are computed under certain assumptions and approximations and a better estimation of their values can lead to some changes to $V(Q_{20})$. (4) The approximations involved in the evaluation of the collective masses can lead to differences with the exact value of the order of 40 or 50%. (5) The pairing correlation is an important ingredient both in the evaluation of the zero-point energy as well as in the evaluation of the collective inertia. As shown below, changes of only a few per cent in the pairing strength values can lead to changes in the theoretical estimation of the half-lives in the range of 5 to 12 orders of magnitude.

On the other hand, the experimental values of the parameters defining the potential energy of the fission process, namely the inner and outer barrier heights and the excitation energy of the fission isomer, are more robust quantities to compare with as they are not as sensitive to pairing correlations as the other parameters. However, these "experimental quantities" are obtained by model-dependent assumptions that can mask the physical meaning of the parameters. Therefore, although we have compared our barrier height values with the experimental ones, we prefer to deal with real observables like the trends in spontaneous fission life times as a function of N and Z.

III. RESULTS

A. Comparison with other interactions

Before comparison with the experimental data, a comparison with the HFB results obtained with the two most commonly used Gogny interactions, namely D1S and D1M, is in order. The Gogny D1S interaction has been used [17] in a thorough study of heavy nuclei properties, including fission, and it has proved to reproduce quite nicely most of the properties analyzed. On the other hand, the fission properties of D1M [45] have not been analyzed in detail, yet but its good behavior regarding other aspects of nuclear structure like binding energies [45], radii [46], quadrupole [47,48], and octupole [49] properties make it a good candidate for comparison. As we have already made comparison [27] with D1S concerning fission properties of actinides (^{240}Pu) and superheavies (^{262}Sg), we will just explore another actinide: the nucleus ^{234}U.

In Fig. 1(a) we compare the HFB energy as a function of Q_{20} for the three functionals in the nucleus ^{234}U. We observe how the shape of the three curves starting at $Q_{20} = 0$ b look rather similar up $Q_{20} = 60$ b, apart from a constant shift of a few MeV. From there on, the D1M interaction declines more gently than D1S. The BCPM results are between D1M and D1S but closer to D1M than to D1S. The decline of energy with increasing quadrupole moment is correlated with the surface energy coefficient in nuclear matter, which is larger in D1M and BCPM than in D1S [27]. The other three curves only present at large Q_{20} values correspond to HFB solutions with two well-separated fragments. They intersect the one-fragment curves at Q_{20} values around 130 b and show a fast quasilinear decrease in energy as the quadrupole moment increases. The charge and mass of each fragment are the ones that lead to the minimum energy for each quadrupole moment. For very large Q_{20} values the distance between the fragments is larger than the range of the nuclear strong interaction and therefore only the Coulomb repulsion energy between the fragments plays a role. In this two-fragment regime the quadrupole moment is directly linked to the separation distance between fragments [43] and therefore increasing the quadrupole moment is equivalent to separating the fragments, in this way reducing the total energy of the system as a consequence of a smaller Coulomb repulsion. Although the two-fragment curves seems to intersect the one-fragment ones, this is just a consequence of projecting out paths in a multidimensional space of collective variables (quadrupole, octupole, hexadecapole, necking, etc.) into a one-dimensional

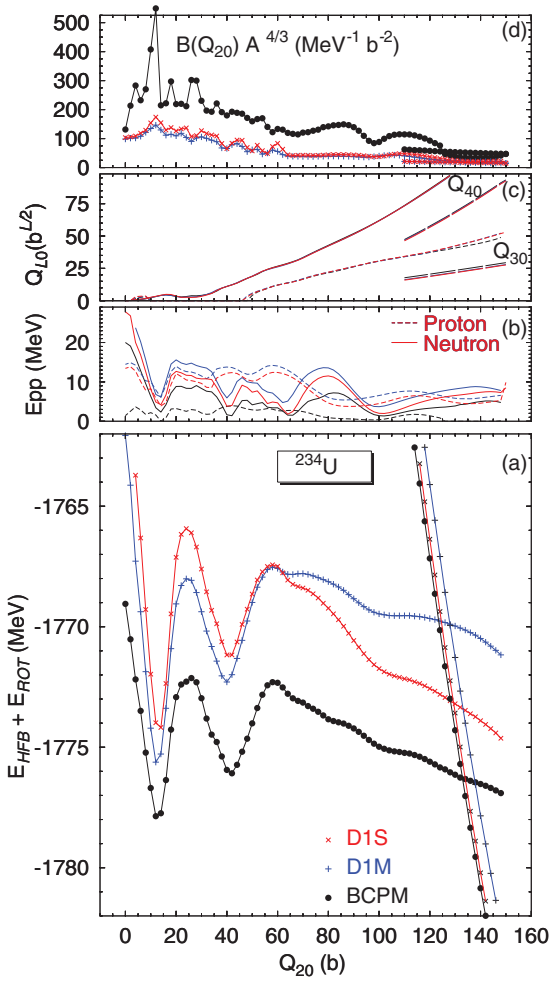

FIG. 1. (Color online) Comparison of mean-field quantities as a function of the mass quadrupole moment Q_{20} for the ^{234}U nucleus. Curves starting at $Q_{20} \approx 120$ b correspond to solutions with two fragments. The BCPM EDF (black line, bullet symbol) as well as the D1S (red times symbol) and D1M (blue plus symbol) parametrizations of the Gogny force are included. In (a) the HFB energy is given. In (b) the particle-particle correlation energy $E_{pp} = -\mathrm{Tr}(\Delta\kappa)$ is plotted for protons (dashed) and neutrons (full) for the three different sets of calculations. In panel (c) the octupole (short dashed) and hexadecapole (full line) moments are given. The two long dashed curves correspond to the two-fragment solutions. Finally, in (d) the ATDHFB collective inertia is depicted.

plot (see below) [50]. There is a minimum action path with a ridge connecting both the one-fragment and the two-fragment curves that goes along the multidimensional space. This path contributes to the action that enters the WKB formula to compute the t_{sf} half-lives. As the determination of this path is cumbersome and its contribution to the action is small, we will neglect its contribution to the action. This simplification amounts to consider both curves as intersecting ones.

A measure of pairing correlations, the pairing interaction energy $E_{pp} = -\mathrm{Tr}(\Delta\kappa)$ is shown as a function of the mass quadrupole moment for protons (dashed lines) and neutrons (full lines) in Fig. 1(b). Again, the shape of the curves looks rather similar for the three functionals but BCPM yields lower values of E_{pp} than D1S and D1M. Those lower values correspond to less intense pairing correlations in the BCPM case with a severe quenching of the proton's pairing correlations. In Fig. 1(c), the octupole and hexadecapole moments as a function of Q_{20} are given. The results for the three EDFs are very similar, to the extent that they appear as a single curve for many Q_{20} values. The full curves correspond to the one-fragment solutions, whereas the long dashed ones correspond to the scissioned configurations. As mentioned before, the values of the multipole moments of the two kinds of curves differ substantially and therefore the paths are quite separated in the multidimensional space of parameters. Finally, in Fig. 1(d), the collective inertia in the ATDHFB approximation is plotted. As in the case of the HFB and particle-particle energies the shape of the curves for the different interactions are quite similar but the BCPM inertia is larger than the inertias obtained with the Gogny forces by up to a factor of three. The large value of the BCPM inertia is a direct consequence of the quenched pairing correlations: Fewer pairing correlations imply a lower gap and therefore smaller two-quasiparticle energies. As the two quasiparticle energies enter the collective inertia in the denominator, quenched pairing correlations imply enlarged collective inertias [4,41]. On the other hand, the D1M inertia is around 15% smaller than the D1S one, consistent again with the quenched pairing correlations in D1M as compared to the D1S ones. The GCM inertias, not depicted, look rather similar in shape to the ATDHFB ones but are a factor of 0.5–0.6 smaller. The inertia for the two-fragment solutions corresponds to the reduced mass of the two fragments [43] and is constant with quadrupole deformation.

In the calculation of the t_{sf} half-life with the WKB formula the configuration with the lowest energy is always chosen. This is an approximation that neglects the path in the multidimensional space that connects the one-fragment solution with the two-fragment solution and therefore the t_{sf} obtained are to be considered as lower bounds. In order to make a more quantitative assessment on the validity of this assumption, we have carried out a calculation where the number of particles in the neck Q_N has been constrained from its value in the one-fragment solution (around 13.5) to the value in the two-fragment case (around 3) and keeping the mass quadrupole moment constant at $Q_{20} = 140$ b. When Q_N decreases the system goes through a ridge around 5 MeV high and located at $Q_N = 5.5$. However, the corresponding collective inertia is small compared to the inertia of the quadrupole degree of freedom and therefore this path connecting the one-fragment with the two-fragment configurations only contributes an extra 8% to the WKB action increasing t_{sf} by 4 orders of magnitude. The choice of the path and collective coordinate is not necessarily optimal and therefore that increase of four orders of magnitude has to be considered as an upper limit.

As is well known, inclusion of triaxiality leads to a reduction of the inner barrier height or the order of one or two MeV. However, the triaxial inertia is larger than the axial one [17], leading to a larger action in the exponent of the WKB formula (see, however, Ref. [51] for another result). As a consequence, the axial path is favored by the dynamics and therefore triaxial effects have not been included in the present calculation. The

values of the t_{sf} half-life obtained for the three EDFs computed with the GCM inertias are $t_{sf} = 2.3 \times 10^{38}$ s, 4.7×10^{29} s, and 1.3×10^{23} s for BCPM, D1M, and D1S, respectively. The large differences observed of up to 15 orders of magnitude can be attributed partly to the difference in the HFB energy curve but mostly to the very different values of the collective inertias. The previous t_{sf} values have been obtained without taking into consideration the reduction of the inner barrier height as a consequence of triaxiality. Also, increasing the value of the E_0 parameter from 1 to 1.5 MeV reduces the half-lives by 6, 2, and 4 orders of magnitude respectively. In any case, the values obtained are several orders of magnitude larger than the experimental value of 4.7×10^{23} s except for Gogny D1S. If the ATDHFB inertias are used instead of the GCM ones, much longer lifetimes are obtained: $t_{sf} = 7.8 \times 10^{52}$ s, 5×10^{40} s, and 2.9×10^{32} s for BCPM, D1M, and D1S, respectively. This tendency to produce longer lifetimes when the ATDHFB inertias are used is common to all the isotopes considered in this study. The ATDHFB inertias are typically a factor 1.5 larger than the GCM ones (see Refs. [40,42] for examples), implying a 20% increase in the action and therefore a 20% increase in the exponent of the penetration factor. This is a source of theoretical uncertainty in the evaluation of t_{sf} that deserves further investigation. Another source of uncertainty comes from the fact that the inertias are computed in the "perturbative cranking approximation," where the energy of elementary excitations is replaced by the sum of HFB quasiparticle energies. This approximation can lead to overestimation in the inertias as large as 40–50% for ground-state configurations [42]. Given the impact of these effects on the fission observables a better quantitative understanding is highly desirable. In the following, to simplify the presentation, we will consider only the GCM inertias in the evaluation of the lifetimes.

In Fig. 2 contour plots of the densities for three values of the quadrupole moment are depicted. They are obtained in calculations with BCPM and differ little from the same quantities computed with D1M and D1S. For the quadrupole moment $Q_{20} = 130$ b, two densities, corresponding to the one-fragment (1F) and two-fragment (2F) solutions, are presented. The two solutions with $Q_{20} = 130$ b have different values of Q_{30} (40.72 $b^{3/2}$ for the 1F solution and 23.44 $b^{3/2}$ for the 2F one) and Q_{40} (99.75 b^2 for the 1F solution and 68.90 b^2 for the 2F one). The two-fragment solution shows a spherical fragment that corresponds to $Z = 51.60$ and $N = 82.00$ and an oblate deformed fragment with $Z = 40.40$ and $N = 60.00$. The non-integer proton and neutron numbers are due to the existence of low density nuclear matter between the two fragments. The oblate and slightly octupole deformed fragment ($\beta_{20} = -0.21$ and $\beta_{30} = 0.03$ acquires this shape to minimize the rather large Coulomb repulsion energy (assuming pointlike fragments, the classical repulsion energy amounts to 196 MeV). This effect has also been observed in other calculations [52,53]. This is an interesting result because it is commonly assumed [50] that the fission fragments only have spheroidal shapes. Coming back to the one-fragment density at $Q_{20} = 130$ b, it is worth mentioning that the number of particles with z between $-\infty$ and 1 fm are $Z = 52.84$ and $N = 82.92$. Increasing the range to 2 fm leads to $Z = 54.35$ and $N = 85.47$. Those are the expected range of Z and N values in the heaviest fragment according to some models of scission [50]. Whether scission takes place according to this scheme or is driven by magic numbers of the fragments is still subject to discussion but the comparison with experimental systematics points to the former explanation as the most likely one.

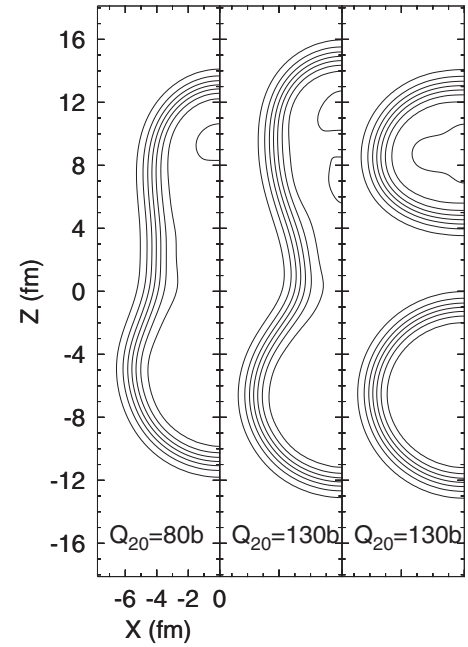

FIG. 2. Contour plot of the total density of ^{234}U for three different configurations along the fission path with quadrupole deformation parameters indicated in each panel. Contour levels correspond to densities between 0.02 and 0.16 fm^3 in steps of 0.02 fm^3. The results correspond to the BCPM EDF.

B. Varying pairing strengths

In the BCPM functional the pairing interaction is taken as a density-dependent contact pairing interaction with strength parameters fixed to reproduce the neutron matter pairing gap of the Gogny force [32]. We have shown in the previous subsection that the particle-particle correlation energy, a quantity related to the amount of pairing correlations, was much smaller for BCPM than for the Gogny forces, leading to much larger collective inertias. It is therefore reasonable to investigate the behavior of fission properties as a function of the pairing strength for the same functional. To this end, a parameter η has been introduced as a multiplicative factor in front of the pairing gap field Δ_{kl}. For the sake of simplicity we have considered a unique parameter for both protons and neutrons, although the use of different parameters will give more flexibility to reproduce the experimental data. The outcome of the calculations with η values of 1.05 and 1.10 for the nucleus ^{234}U are presented in Fig. 3. We observe in Fig. 3(a) that increasing the pairing strength by 10% ($\eta = 1.10$) leads to an overall gain of the order of 1 MeV in binding energy. For the ground state this 1-MeV energy gain has to be compared to the 1 MeV of pairing correlation energy for the standard BCPM. The gain is even larger (1.6 MeV) for

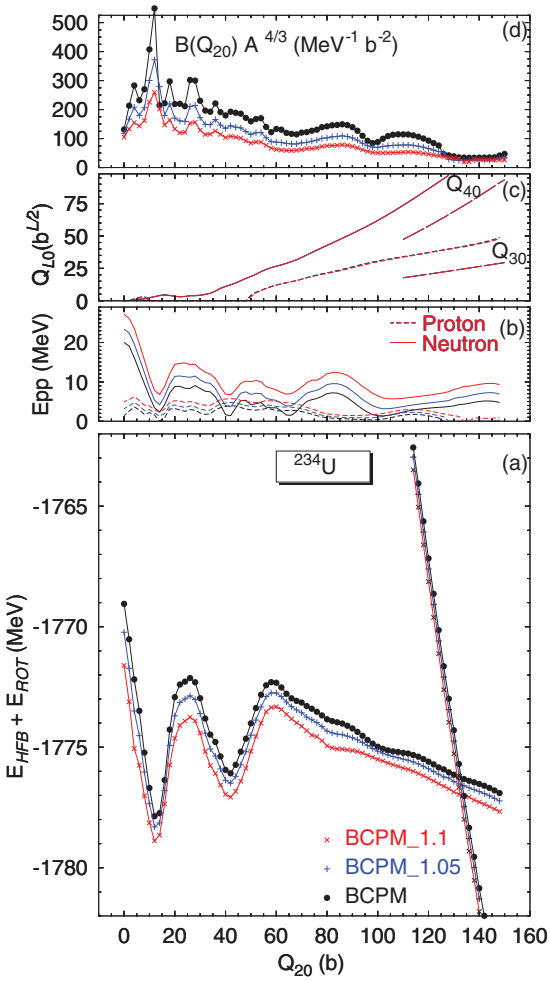

FIG. 3. (Color online) Same as shown in Fig. 1 but for different pairing strengths. The pairing strengths are given in terms of the reference value and a scaling parameter η taking the values 1.00 (the standard calculation), 1.05, and 1.10.

the configuration with $Q_{20} = 26$ b and corresponding to the top of the inner barrier. However, the standard BCPM pairing correlation energy is 2.06 MeV for that configuration. The net effect of increasing the pairing strength by 10% is to decrease the inner barrier eight ($B_{\rm I}$) by 0.6 MeV, whereas the other parameters, namely the outer barrier height $B_{\rm II}$ and the fission isomer excitation energy, remain more or less the same. The particle-particle correlation energies E_{pp} shown in Fig. 3(b) for protons and neutrons increase with increasing η but the slope is larger for neutrons than for protons. The multipole moment values depicted in Fig. 3(c) do not change at all when the pairing strength is increased and the different values lie on top of each other for different η values. Finally, the impact on the collective inertia is clearly visible in Fig. 3(d) and is associated to the inverse dependence of the mass on the square of pairing gap [4,41]. Increasing the pairing strength by 5% reduces the collective inertia by roughly 30% whereas a 10% increase leads to a reduction of 50%. The consequences of these reductions on the $t_{\rm sf}$ are dramatic, decreasing its value by 11 orders of magnitude in going from $\eta = 1.0$ to $\eta = 1.05$ ($t_{\rm sf} = 8.0 \times 10^{27}$ s) and six additional orders of magnitude in going from $\eta = 1.05$ to $\eta = 1.10$ ($t_{\rm sf} = 6.7 \times 10^{21}$ s). This result is a clear indication of the very important role played by pairing correlations in the description of fission. The result suggests that experimental fission data could be used to fine-tune the pairing strength instead of more traditional approaches based on odd-even staggering. From a theoretical perspective, the result also points to the very important role that the correlations associated to particle number symmetry restoration should have in fission dynamics. Restoring particle number symmetry usually leads to larger pairing correlations than the ones present at the mean-field level and therefore will have a tremendous impact on fission lifetimes. In this respect it is worth mentioning that the dependence on density of BCPM is on integer powers of the density, allowing the use of the regularization techniques suggested to solve some technical problems associated to the evaluation of the energy kernel overlaps required by symmetry restoration theories (see Refs. [56,57] and references therein).

Given the large variability of the lifetimes with the different parameters entering the WKB formula, a direct comparison with the experimental data is meaningless and only comparisons with the trends along a series of nuclei or isotopes, all of them computed in the same conditions, can lead to meaningful conclusions regarding fission properties.

C. Nuclei with known experimental data

In order to validate BCPM as a functional able to describe fission properties, we have performed calculations for those even-even nuclei where the spontaneous fission half-life has been measured. We will also compare the parameters defining the theoretical potential energy surface, namely the inner and outer barrier heights ($B_{\rm I}$ and $B_{\rm II}$) and the excitation energy of the fission isomer $E_{\rm II}$ with available experimental data [54,55]. It has to be mentioned that the experimental data for $B_{\rm I}$ and $B_{\rm II}$ [55] is model dependent and therefore less reliable that the pure $t_{\rm sf}$ data. In Table I the experimental and theoretical values for $B_{\rm I}$, $B_{\rm II}$, and $E_{\rm II}$ are given for all nuclei where experimental data exist [54,55]. The theoretical values have been obtained by considering the HFB energy as a function of Q_{20} with the rotational energy correction (computed in the way described in the previous section) subtracted. The effect of the zero-point energy correction $\epsilon_0(Q_{20})$ has not been included, mainly because it is almost constant as a function of Q_{20}. We notice that the theoretical predictions for $B_{\rm I}$ are typically one or two MeV larger than experiment. This is not surprising as it is well known that the theoretical inner fission barrier is affected by triaxiality and its height typically decreases by one or two MeV when the effect is included in the calculation [17]. Triaxiality is not included at present because we still do not have access to a triaxial code incorporating the BCPM functional but work in this direction is in progress. The situation is slightly better in the comparison with the $E_{\rm II}$ and $B_{\rm II}$ values. For them, no significant triaxial effects are expected and the agreement with experiment is better than for the B_I. In Ref. [9] a thorough comparison of these data with various model predictions has been made. In that paper, the rms deviations for the fission isomer energy and second barrier height are given for several mean-field models. The BCPM values $\sigma(E_{\rm II}) = 0.57$ MeV

TABLE I. Fission barrier height parameters $B_{\rm I}$ (inner) and $B_{\rm II}$ (outer) as well as excitation energy of the fission isomer $E_{\rm II}$. The three parameters are given in MeV. The theoretical values have been obtained from the rotational energy corrected HFB potential energy surface. The experimental values are taken from [54] for the $E_{\rm II}$ and from [55] for the B's.

Nucleus	$B_{\rm I}^{\rm Th}$	$E_{\rm II}^{\rm Th}$	$B_{\rm II}^{\rm Th}$	$B_{\rm I}^{\rm Exp}$	$E_{\rm II}^{\rm Exp}$	$B_{\rm II}^{\rm Exp}$
^{234}U	5.87	1.78	5.59	4.80	–	5.50
^{236}U	6.49	1.90	6.04	5.0	2.75	5.67
^{238}U	6.99	2.03	6.54	6.30	2.55	5.50
^{238}Pu	6.91	1.85	5.20	5.60	2.4	5.10
^{240}Pu	7.43	2.08	5.69	6.05	2.8	5.15
^{242}Pu	7.72	2.27	6.30	5.85	2.2	5.05
^{244}Pu	7.89	2.47	6.30	5.70	–	4.85
^{240}Cm	6.8	1.2	3.90	–	2	–
^{242}Cm	7.4	1.7	4.5	6.65	1.9	5.0
^{244}Cm	8.0	1.9	5.0	6.18	2.2	5.10
^{246}Cm	8.4	2.3	5.5	6.0	–	4.80
^{248}Cm	8.34	2.04	5.47	5.80	–	4.80
^{250}Cf	8.65	1.25	4.24	–	–	3.8
^{252}Cf	8.35	0.83	3.84	–	–	3.5

and $\sigma(B_{\rm II}) = 0.72$ MeV are similar in magnitude to the ones of UNEDF1 [8], a Skyrme variant specifically tailored to describe fission. This is a quite satisfactory result, taking into account that BCPM does not use any fission data in its fit.

In Fig. 4 the theoretical $t_{\rm sf}$ results obtained for different choices of the E_0 and η parameters are compared to the known experimental values. The experimental $t_{\rm sf}$ values [58] span a range of 27 orders of magnitude for a mass range $A = 232$–286. The theoretical predictions, not including triaxial effects

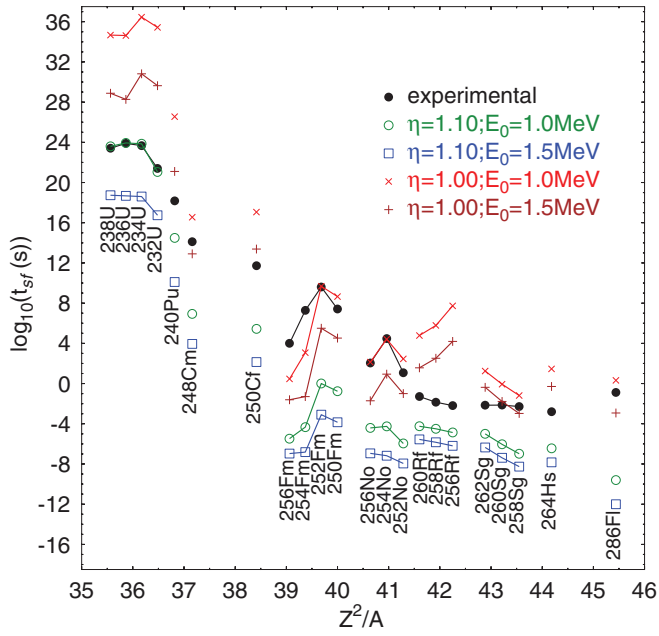

FIG. 4. (Color online) Experimental $t_{\rm sf}$ half-lives (bullets) are compared to different theoretical results (open symbols) for several isotopic chains where experimental data exists. The $t_{\rm sf}$ are plotted as a function of the fissibility parameter Z^2/A. See text for details.

and computed with the GCM masses and zero-point energies, span an even larger range of values and show a large variability depending upon the choices for the parameters. Focusing on the "standard" theoretical values $\eta = 1.0$ and $E_0 = 1.0$ we observe differences with the experiment of up to 16 orders of magnitude for the lighter nuclei that steadily decrease to differences of just a couple of orders of magnitude for the heavier ones. The largest differences are observed for nuclei with higher and wider barriers where the impact of parameters like E_0 is larger. The comparison in isotopic chains indicate that the trend with neutron number compares much better with the experiment than the absolute values. The same conclusion can be drawn for the overall trend with mass number as can be inferred from the plot. Therefore, we conclude that the HFB predictions, although subject to large uncertainties due to uncontrolled approximations in the evaluation of the different parameters, can be used to estimate with reasonable confidence the trends of $t_{\rm sf}$ with mass number. The second conclusion drawn from this plot is the extreme sensitivity of the half-lives to changes in η and E_0: Increasing the pairing strength by 10% ($\eta = 1.10$) decreases $t_{\rm sf}$ by several orders of magnitude. In the uranium isotopes the reduction is of 12 orders of magnitude, bringing the theoretical predictions on top of the experimental data. On the contrary, in the Fm and No isotopic chains the reduction represents only 6 orders of magnitude but worsens the agreement with experiment. On the other hand, the increase of E_0 from 1 to 1.5 MeV also reduces $t_{\rm sf}$ by several orders of magnitude, but the reduction is not as severe as with the increase of pairing strength. In the uranium case, the reduction represents on the average 6 orders of magnitude. Incidentally, the $t_{\rm sf}$ values obtained with $\eta = 1$ and $E_0 = 1.5$ MeV are in most of the cases very close to the results (not shown) corresponding to $\eta = 1.05$ and $E_0 = 1$ MeV.

The sensitivity of the results to the pairing strength demands a theory beyond HFB to describe pairing correlations. A first candidate would be particle number restoration supplemented with configuration mixing using the pairing gaps as collective coordinates. Also the sensitivity to the E_0 parameter justifies an effort to better understand its rationale. This is obviously a task for the future.

Another important piece of relevant information is the mass distribution of the fission fragments. The mass of the fragments is determined by the nuclear shape in the neighborhood of the scission point. As the scission point is difficult to characterize in a mean-field theory that explores just a few degrees of freedom, we have preferred to take a different approach that involves the evaluation of quasifusion configurations. They are obtained by constraining the number of particles in the neck of the parent nucleus,

$$Q_N = \langle\phi|\hat{Q}_N(z_0, C_0)|\phi\rangle,$$

to a small value and then releasing the constraint to do a self-consistent calculation. Most of the time the self-consistent solution ends up in a solution with two well-separated fragments. To make sure that the configuration is the lowest in energy the procedure is repeated with different choices of the neck operator parameters z_0 (position of the neck along the z direction) and C_0 (the width of the neck distribution). Those configurations are constrained to larger quadrupole

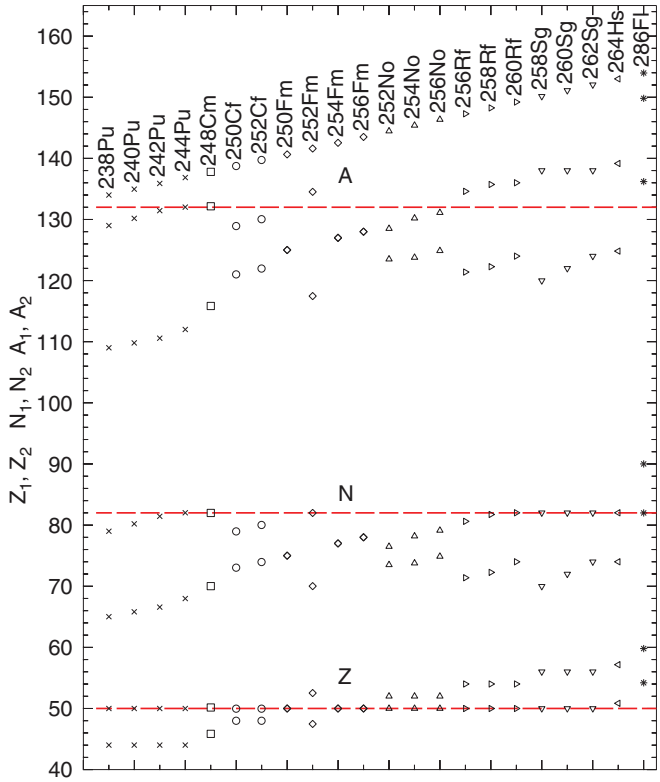

FIG. 5. (Color online) Proton ($Z_{1,2}$), neutron ($N_{1,2}$), and mass number ($A_{1,2}$) of the two fragments emitted by the fission of the parent actinides (perpendicular labels on top). The magic numbers 50 and 82 as well as its sum are highlighted with horizontal lines.

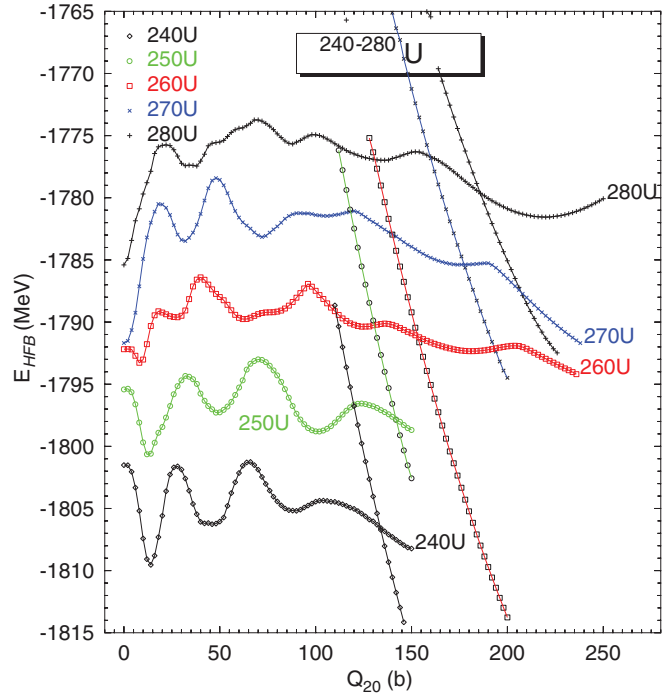

FIG. 6. (Color online) HFB energies as a function of the quadrupole moment Q_{20} for some neutron-rich uranium isotopes. The energies have been shifted upwards for the heavier isotopes in order to fit all the curves in a single plot. Along with the one-fragment curves starting at $Q_{20} = 0$ the curves corresponding to the energy of the two fragments resulting in fission are given.

moments in order to separate the fragments (please remember that for two fragments the quadrupole moment is proportional to the separation of the fragments [43]). An example of those quasifusion curves has already been presented in Fig. 1. In Fig. 5 the proton (Z) and neutron (N) numbers of the fragments obtained for the actinides considered are given. The Z values of the fragments are mostly determined by the $Z = 50$ magic number except in ^{252}Fm. Also for the heaviest nucleus considered $^{266}_{114}$Fl larger Z values are observed. For neutrons, the magic $N = 82$ seems also to be dominant neutron number but here the exceptions are more numerous. For the plutonium and heavier isotopes the heaviest fragment has a mass number between 130 and 132, 10 units less than the average experimental value of Refs. [59,60]. The discrepancy can be attributed to the lack of quantum fluctuations in our model that can modify substantially the raw mean-field numbers [16].

Obviously, the numbers given here are meant to represent the peaks of the fragments' mass distribution, which is a broad distribution as a consequence of exchange of particles during the scission process as well as a consequence of neutron evaporation. A better dynamical theory is required (see Ref. [16] as an example of such theory) in order to reproduce the experimental broad distribution.

D. Neutron-rich uranium isotopes

In the previous section we concluded that the description of fission based on the HFB theory is subject to large uncertainties coming from the poor understanding of the way the different quantities entering the WKB formula should be determined. However, we also concluded that the HFB theory is reproducing reasonably well the experimental t_{sf} trends with mass number. Encouraged by the result, we have performed calculations in the uranium isotopic chain from the light uranium ^{226}U up to the neutron drip line corresponding to ^{282}U with the aim of understanding and analyzing the trends in spontaneous fission half-lives and the mass of the emerging fission fragments. To illustrate the results, the HFB potential energies for the ^{240}U, ^{250}U, ^{260}U, ^{270}U, and ^{280}U isotopes are depicted as a function of Q_{20} in Fig. 6. The energies of the heavier isotopes have been shifted by different amounts (55, 100, 135, and 160 MeV, respectively) to fit all the curves in a single plot. In addition, the curves corresponding to the two-fragment solution with the lowest energy are depicted.

We observe the ground-state evolution from a quadrupole deformed ground state in ^{240}U with $\beta_{20} = 0.26$ to a spherical one for ^{270}U (corresponding to $N = 178$) and for ^{280}U. It is also worth mentioning the existence of a second fission isomer in ^{240}U (excitation energy of 3.9 MeV) and ^{250}U (excitation energy of 3.8 MeV, lower than the excitation energy of the first isomer). The situation in ^{260}U is not as well defined as in the previous cases as there are three very swallow minima. The second one could be associated to the first fission isomer that is shifted to larger quadrupole moment values and zero octupole moment. Two fission isomers reappear in ^{270}U but both are located at a very high excitation energy (around 9 MeV) and

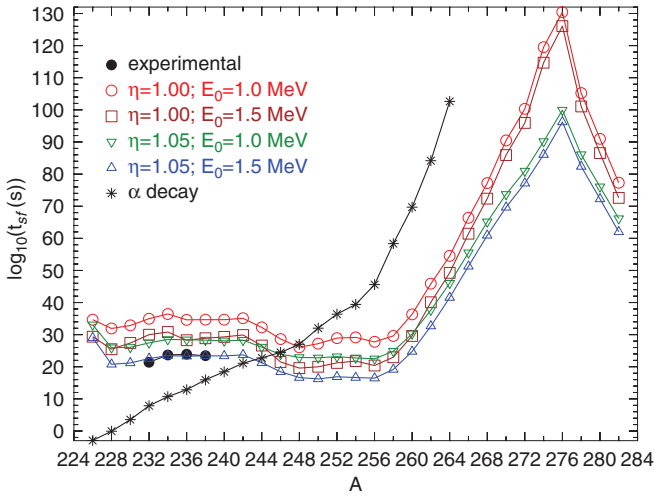

FIG. 7. (Color online) Experimental t_{sf} half-lives (bullets) are compared to different theoretical results (open symbols, fission; asterisk α decay) for the uranium isotopes up to the drip line nucleus ^{282}U.

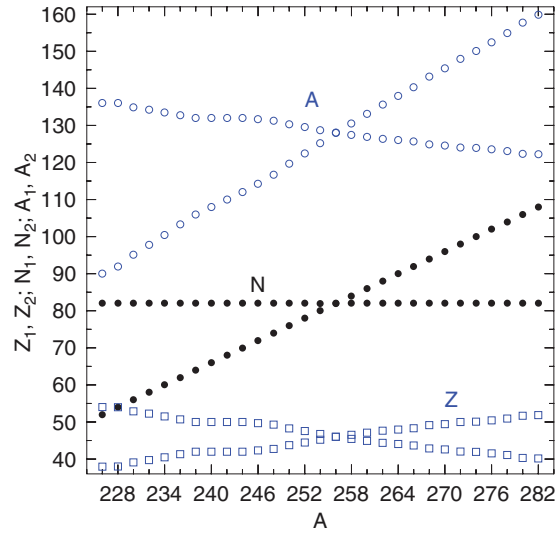

FIG. 8. (Color online) The number of protons ($Z_{1,2}$), neutrons ($N_{1,2}$), and mass number ($A_{1,2}$) of the fission fragments is plotted as a function of the mass number A of the parent uranium isotope.

different quadrupole deformations than the ones in the light uranium isotopes. As a consequence of the increasing height and widening of the fission barriers as the neutron number approaches the neutron drip line, we expect increasing t_{sf} values. Our fission barrier heights are consistent with the semiclassical values obtained in Ref. [61] and remarkably differ from the macroscopic-microscopic model predictions discussed in that paper. Both our results and the semiclassical Thomas Fermi results of Ref. [61] support enhanced stability against fission as the neutron drip line is approached. In Fig. 7 the spontaneous fission half-lives t_{sf} of the uranium isotopes computed with different choices of the η and E_0 parameters are plotted as a function of mass number A. Like the previous cases, the t_{sf} values have been obtained with the GCM collective mass and not taking into account the effects of triaxiality in the first barrier. The usual range of up to 12 orders in magnitude depending on the choice of parameters is observed. However, the trend with mass number A is the same in all the four sets of parameters considered. This again gives us confidence in the validity of the conclusions extracted from the trends with mass number. A decrease in the t_{sf} values is observed up to mass number $A = 256$, where the trend changes to a steady increase with mass number up to ^{276}U, where the t_{sf} values reach a maximum that corresponds to a neutron number of 184 that is precisely one of the predicted magic numbers in the superheavy region (see Ref. [62] for a discussion and other predictions). The two neutron separation energy drops by 3 MeV in going from $A = 276$ (4.99 MeV) to $A = 278$ ($S_{2N} = 1.94$ MeV), indicating extra stability. The half-lives for this and the other isotopes beyond ^{260}U are very large and the corresponding nuclei can be considered as stable against the spontaneous fission decay channel. As the BCPM functional has been created to provide a reasonable description of masses, it is reasonable to use its predictions for the binding energies of uranium and thorium to compute the half-lives of α decay using the phenomenological Viola-Seaborg formula [63,64]. The results for the uranium isotopes are plotted as asterisks in the figure. We observe a steady increase of t_α with mass number that reaches its maximum at $A = 264$, where α decay is no longer favorable energetically. From $A = 244$ on fission is faster than α decay.

In Fig. 8 the proton, neutron, and mass numbers of the fragments in the fission of the uranium isotopes are plotted as a function of mass number A. Those numbers are obtained by integrating the densities of each of the fragments coming out of the two-fragment (fusion valley) self-consistent solutions mentioned before and corresponding to the lowest energy. They do not take into account the dynamics of rupture in the scission point that determines the fate of the protons and neutrons present in the neck prior to scission. In some cases, there are additional fusion valleys with different masses of the fragments but they lie higher in energy. The issue of how to describe dynamically the evolution of the system through those valleys is a very interesting subject of research (see, for instance, Ref. [16]) with many practical applications (the real fission fragment mass distribution) but exceeds the scope of the present paper. The numbers discussed below are to be taken as a rough indication of the peaks (most favorable mass) of the mass distribution of fragments prior to neutron emission. For all the nuclei considered, the number of neutrons in one of the fragments always corresponds to the magic number $N = 82$. The neutron number of the other fragment varies linearly accordingly to the mass number of the parent. On the other hand, the number of protons, that is close to the magic number $Z = 50$ for the light isotopes (in good agreement with experiment [65]) varies linearly with mass number except for the isotopes $^{238-244}$U, where it stabilizes at $Z = 50$. For the ^{256}U isotope a symmetric splitting with equal fragments ($Z = 46$ and $N = 82$) is obtained. Concerning the mass distribution of the fragments, the heavy fragment has a mass number around 136 for the light isotopes that decreases with the mass number of the parent until the ^{256}U isotope is reached. At this point the mass number of the heavy isotope starts to increase linearly. This change in tendency is due to the increasing

number of neutrons: as the number of neutrons increases, the fragment with $N = 82$ is no longer the heaviest one.

IV. CONCLUSIONS

The fission properties of several actinides and superheavy nuclei have been computed with the recently proposed BCPM EDF. The theoretical results for the spontaneous fission half-lives show a large variability consequence of uncertainties in the evaluation of some parameters of the theory and also on the strong dependence of the collective inertia with pairing correlations. As a consequence of the large uncertainties in the theoretical results we are only able to compare with the experimental data trend with mass number (for instance, the reduction by 27 orders of magnitude in the spontaneous fission half-lives in going from $A = 232$ to $A = 286$). The theoretical predictions seem to reproduce such a trend, giving us confidence in the convenience of the method and EDF for the study of fission properties of neutron-rich uranium isotopes. There we find that the spontaneous fission half-lives remain more or less constant up to $A = 260$, where they increase enormously as a consequence of the proximity to the magic neutron number $N = 184$. Therefore, it is confirmed the prevalence of this magic number in a extreme neutron-rich case. On the other hand, a comparison of the parameters defining the potential energy surface for fission (inner and outer barrier heights and fission isomer excitation energies) with the model-dependent "experimental data" show a rather good agreement that gives us additional confidence on the validity of our conclusions. The results obtained clearly show that more attention has to be paid to a proper description (including beyond-mean-field effects) of pairing correlations in the configurations relevant to fission. The evaluation of the quasifission valley in the HFB model also allows us to predict the peaks of the mass distribution of fission fragments. It is shown that the magic proton number $Z = 50$ and the magic neutron number $N = 82$ play an important role in determining the mass of the fragments.

To conclude, our study has shown the applicability of the BCPM EDF for fission studies in heavy and superheavy nuclei. We have also pointed out the large variability of the theoretical predictions to the models used to evaluate the relevant parameters. However, this variability seems to respect the trend with mass number of the spontaneous fission half-life and therefore we have applied our method to study fission properties of the uranium isotopes up to the neutron drip line. It is shown that beyond $A = 264$ the uranium isotopes can be considered as stable against fission and α decay.

ACKNOWLEDGMENTS

Work supported in part by MICINN Grants No. FPA2012-34694 and No. FIS2012-34479 and by the Consolider-Ingenio 2010 program MULTIDARK CSD2009-00064.

[1] H. J. Krappe and K. Pomorski, *Theory of Nuclear Fission*, Lecture Notes in Physics Vol. 838 (Springer, Berlin, 2012).
[2] D. N. Poenaru, *Nuclear Decay Modes* (Institute of Physics, Bristol, UK, 1996).
[3] Hans J. Specht, Rev. Mod. Phys. **46**, 773 (1974); S. Björnholm and J. E. Lynn, *ibid.* **52**, 725 (1980); Nucl. Phys. A **502**(1) (1989).
[4] M. Brack, J. Damgaard, A. S. Jensen, H. C. Pauli, V. M. Strutinsky, and C. Y. Wong, Rev. Mod. Phys. **44**, 320 (1972).
[5] J. Decharge and D. Gogny, Phys. Rev. C **21**, 1568 (1980).
[6] J. F. Berger, M. Girod, and D. Gogny, Nucl. Phys. A **428**, 23 (1984).
[7] J. Bartel, P. Quentin, M. Brack, C. Guet, and H. B. Häkansson, Nucl. Phys. A **386**, 79 (1982).
[8] N. Nikolov, N. Schunck, W. Nazarewicz, M. Bender, and J. Pei, Phys. Rev. C **83**, 034305 (2011).
[9] J. McDonnell, N. Schunck, and W. Nazarewicz, arXiv:1301.7587 [nucl-th].
[10] P. Ring and P. Schuck, *The Nuclear Many-Body Problem* (Springer-Verlag, Berlin, 1980).
[11] M. Bender, P.-H. Heenen, and P.-G. Reinhard, Rev. Mod. Phys. **75**, 121 (2003).
[12] J. Erler, K. Langanke, H. P. Loens, G. Martínez-Pinedo, and P.-G. Reinhard, Phys. Rev. C **85**, 025802 (2012).
[13] A. Staszczak, A. Baran, and W. Nazarewicz, Phys. Rev. C **87**, 024320 (2013).
[14] J. L. Egido and L. M. Robledo, Phys. Rev. Lett. **85**, 1198 (2000).
[15] M. Warda, J. L. Egido, L. M. Robledo, and K. Pomorski, Phys. Rev. C **66**, 014310 (2002); Int. J. Mod. Phys. E **13**, 169 (2004).
[16] H. Goutte, J. F. Berger, P. Casoli, and D. Gogny, Phys. Rev. C **71**, 024316 (2005).
[17] J.-P. Delaroche, M. Girod, H. Goutte, and J. Libert, Nucl. Phys. A **771**, 103 (2006).
[18] N. Dubray, H. Goutte, and J.-P. Delaroche, Phys. Rev. C **77**, 014310 (2008).
[19] V. Martin and L. M. Robledo, Int. J. Mod. Phys. E **18**, 788 (2009).
[20] S. Perez-Martin and L. M. Robledo, Int. J. Mod. Phys. E **18**, 861 (2009).
[21] W. Younes and D. Gogny, Phys. Rev. C **80**, 054313 (2009).
[22] H. Abusara, A. V. Afanasjev, and P. Ring, Phys. Rev. C **82**, 044303 (2010).
[23] B. N. Lu, E. G. Zhao, and S. G. Zhou, Phys. Rev. C **85**, 011301 (2012).
[24] A. V. Afanasjev and O. Abdurazakov, Phys. Rev. C **88**, 014320 (2013).
[25] G. Martinez-Pinedo, D. Mocelj, N. T. Zinner, A. Kelić, K. Langanke, I. Panov, B. Pfeiffer, T. Rauscher, K.-H. Schmidt, and F.-K. Thielemann, Prog. Part. Nucl. Phys. **59**, 199 (2007).
[26] I. V. Panov, I. Yu. Korneev, G. Martinez-Pinedo, and F.-K. Thielemann, Astr. Lett. **39**, 150 (2013).
[27] M. Baldo, L. M. Robledo, P. Schuck, and X. Viñas, Phys. Rev. C **87**, 064305 (2013).
[28] M. Baldo, P. Schuck, and X. Viñas, Phys. Lett. B **663**, 390 (2008).
[29] M. Baldo, L. M. Robledo, P. Schuck, and X. Viñas, J. Phys. G **37**, 064015 (2010).
[30] L. M. Robledo, M. Baldo, P. Schuck, and X. Viñas, Phys. Rev. C **77**, 051301(R) (2008).

[31] L. M. Robledo, M. Baldo, P. Schuck, and X. Viñas, Phys. Rev. C **81**, 034315 (2010).
[32] E. Garrido, P. Sarriguren, E. Moya de Guerra, and P. Schuck, Phys. Rev. C **60**, 064312 (1999).
[33] M. Baldo, C. Maieron, P. Schuck, and X. Viñas, Nucl. Phys. A **736**, 241 (2004).
[34] G. Taranto, M. Baldo, and G. F. Burgio, arXiv:1302.6882 [nucl-th].
[35] L. M. Robledo, HFBAXIAL computer code (2002).
[36] L. M. Robledo and G. F. Bertsch, Phys. Rev C **84**, 014312 (2011).
[37] M. Girod and B. Grammaticos, Nucl. Phys. A **330**, 40 (1979).
[38] M. J. Giannoni and P. Quentin, Phys. Rev. C **21**, 2060 (1980); **21**, 2076 (1980).
[39] J. Libert, M. Girod, and J.-P. Delaroche, Phys. Rev. C **60**, 054301 (1999).
[40] A. Baran, J. A. Sheikh, J. Dobaczewski, W. Nazarewicz, and A. Staszczak, Phys. Rev. C **84**, 054321 (2011).
[41] G. F. Bertsch and H. Flocard, Phys. Rev. C **43**, 2200 (1991).
[42] J. L. Egido and L. M. Robledo, Lect. Notes Phys. **641**, 269 (2004).
[43] M. Warda and L. M. Robledo, Phys. Rev. C **84**, 044608 (2011).
[44] A. Baran, Z. Lojewski, K. Sieja, and M. Kowal, Phys. Rev. C **72**, 044310 (2005).
[45] S. Goriely, S. Hilaire, M. Girod, and S. Perú, Phys. Rev. Lett. **102**, 242501 (2009).
[46] R. Rodríguez-Guzmán, P. Sarriguren, L. M. Robledo, and S. Perez-Martin, Phys. Lett. B **691**, 202 (2010).
[47] L. M. Robledo, R. R. Rodríguez-Guzmán, and P. Sarriguren, Phys. Rev. C **78**, 034314 (2008).
[48] R. Rodriguez-Guzman, P. Sarriguren, L. M. Robledo, and J. E. Garcia-Ramos, Phys. Rev. C **81**, 024310 (2010).
[49] L. M. Robledo and G. F. Bertsch, Phys. Rev. C **84**, 054302 (2011).
[50] P. Moller, A. J. Sierk, T. Ichikawa, A. Iwamoto, R. Bengtsson, H. Uhrenholt, and S. Aberg, Phys. Rev. C **79**, 064304 (2009).
[51] J. Sadhukhan, K. Mazurek, A. Baran, J. Dobaczewski, W. Nazarewicz, and J. A. Sheikh, arXiv:1310.2003 [nucl-th].
[52] M. Warda, K. Pomorski, J. L. Egido, and L. M. Robledo, J. Phys. G: Nucl. Part. Phys. **31**, S1555 (2005).
[53] M. Warda, K. Pomorski, J. L. Egido, and L. M. Robledo, Int. J. Mod. Phys. E **14**, 403 (2005).
[54] B. Singh, R. Zywina, and R. Firestone, Nucl. Data Sheets **97**, 241 (2002).
[55] R. Capote *et al.*, Nucl. Data Sheets **110**, 3107 (2009).
[56] L. M. Robledo, Int. J. Mod. Phys. E **16**, 337 (2007).
[57] L. M. Robledo, J. Phys. G **37**, 064020 (2010).
[58] N. E. Holden and D. C. Hoffman, Pure Appl. Chem. **72**, 1525 (2000).
[59] D. C. Hoffman and M. M. Hoffman, Annu. Rev. Nucl. Sci. **24**, 151 (1974).
[60] L. Dematté, C. Wagemans, R. Barthélémy a, R. D'hondt, and A. Deruytter, Nucl. Phys. A **617**, 331 (1997).
[61] A. Mamdouh, J. M. Pearson, M. Rayet, and F. Tondeur, Nucl. Phys. A **679**, 337 (2001).
[62] T. Sil, S. K. Patra, B. K. Sharma, M. Centelles, and X. Viñas, Phys. Rev. C **69**, 044315 (2004).
[63] V. E. Viola, Jr. and G. T. Seaborg, J. Inorg. Nucl. Chem. **28**, 741 (1966).
[64] T. Dong and Z. Ren, Eur. Phys. J. A **26**, 69 (2005).
[65] K.-H. Schmidt *et al.*, Nucl. Phys. A **665**, 221 (2000).